Carbon Trends 15 (2024) 100339

Contents lists available at ScienceDirect

Carbon Trends

journal homepage: www.elsevier.com/locate/cartre

Synthesis and characterization of graphene oxide (GO) for the removal of lead ions in water

L.S. Mokoena *, J.P. Mofokeng *

Department of Chemistry, University of the Free State, (QwaQwa campus), Kestell road, QwaQwa, Phuthaditjhaba, 9866, South Africa

ARTICLE INFO

Keywords:
Graphene oxide
Expandable graphite
Morphology
Adsorption
Isotherm modelling

ABSTRACT

The synthesis and characterization of graphene oxide (GO) for water related applications has become an increasing area of research. GO was prepared via Hummer's method, and analysed for structure, morphology, thermal stability, and the ability to remove heavy lead ions from solution. In FTIR analyses, hydroxyl, carboxyl and ester groups were found to be on the structure of GO. XRD showed the interlayer spacing to have increased from graphite to graphene oxide, whereby the average crystallite size of GO was 16.13. Then SEM confirmed the morphology of GO to be exfoliated and wrinkled, with stacked layers. In TGA, EG degraded in a single step, while GO degraded in three distinct steps. When using AAS to analyse the Pb (II) ion intake properties of GO, it showed a maximum adsorption of 98.1% for 600 ppm lead ion solution. The Freundlich isotherm model was consistent with this adsorption, meaning that adsorption took place on a heterogenous surface, on a multilayer basis. The value of n for this isotherm was 0.1474, implying a dominant chemical adsorption. A significant contribution was done to the structure of GO, with its metal adsorption properties clearly portrayed.

1. Introduction

Graphene oxide (GO) has been one of the major materials of interest on a global scale, due to its unique properties that are of importance in different applications. Over the years different researchers have explored the properties of this material, however, there really has not been one acceptable molecular formula and structure for GO [1].

A variety of proposed structures for GO exist today, and Hofmann and Rudolph [2] were the first to suggest how the structure is, in 1939. In their model, they postulated that numerous epoxy groups were randomly distributed across the singular layer of graphite. Then Ruess [3] provided an alteration to the model in 1946, through the incorporation of hydroxyl groups to GO, as well as having the sp^2 hybridized carbons alternate with those that are sp^3 hybridized. From there came Scholz and Boehm [4] in 1969, who proposed that the structure should be less organized with the presence of C = C bonds. Their structure suggested that there are C—C bonds that occur in a periodic manner in the layers of GO, and these bonds are ridged with carbonyl and hydroxyl groups, with no ether groups. Then some time passed until 1994, whereby Nakajima and Matsuo [5] emerged, to just propose that the GO has a structure comprising of intercalated graphite in it. Shortly after that, in 1998, another model was created by Lerf and Klinowski, called the LK model [6]. In this model, GO was described in terms of two regions: One where there are six membered aliphatic rings, and another where there are benzene rings that are not oxidized. The extent to which the material is oxidized determines the sizes of these regions, and this model describes the presence of mostly epoxide groups, aromatic rings, and double bonds on GO. Wrinkling in the monolayer of GO was also described in this model, and it was said to be due to the slight extortion of hydroxyl groups attached to carbon, in their tetrahedral configuration. This means that the visibility of wrinkles on the microscopical analyses of GO could imply the presence of hydroxyl groups, according to this model. It would further suggest that the attachment of oxygen containing functional groups on the monolayer of GO, occurs on the top and bottom of the layer creating two layers of these groups. The said groups are mainly the hydroxyls and the epoxides, situated very closely to each other and attached to the edges of the GO lattice. Then the other groups of oxygen, oxidized rings and aromatic substances are said to be randomly distributed across the singular layer of carbon.

To this day, the l-K model has formed part of the widely accepted models for the typical structure of graphene oxide. Fig. 1 below shows a representation of graphene oxide which depicts the distribution and presence of its groups, according to this model.

From there, various researchers came with their variations of this

* Corresponding authors.
E-mail addresses: lesiamokoena8@gmail.com (L.S. Mokoena), mofokengJP@ufs.ac.za (J.P. Mofokeng).

https://doi.org/10.1016/j.cartre.2024.100339
Received 22 September 2023; Received in revised form 8 March 2024; Accepted 8 March 2024
Available online 16 March 2024

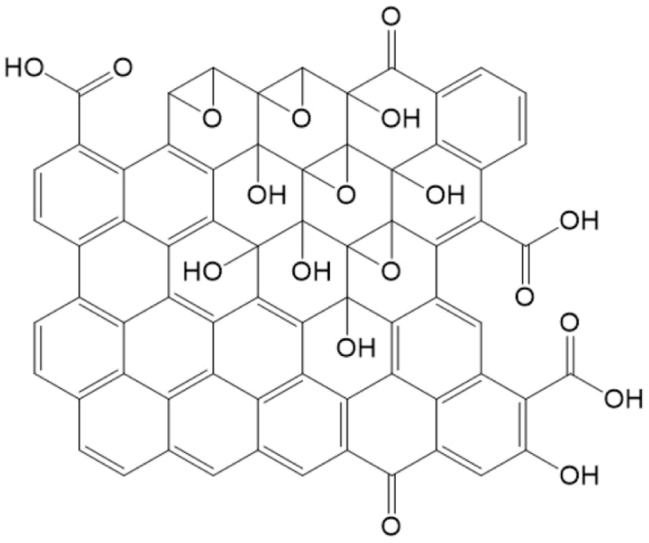

Fig. 1. The proposed L-K model of graphene oxide [7].

model, and the l-K model was partially confirmed. It is thus very evident that there is a gap in the exploration of the structure of GO, that needs to be filled. Any contribution would therefore suffice and move us a step further into understanding, fully, the molecular structure of GO, as well as its surface properties.

The need to fully understand the structure of GO would enable the assessment of its feasibility in being used in different applications. Specifically, the contamination of water by heavy metals remains rife, and the oxygen-containing functional groups on GO could help alleviate this. In our recent publication [8], we reviewed the recent strides made in the structure and properties of graphene oxide and its polymeric composites, for specific purposes of removing heavy metals from water. The work demonstrates the effectiveness of GO in removing heavy metals from water through the process of adsorption and the setbacks thereof. As we know, heavy metal ions form part of the major pollutants in water on global scale, and their effective removal is thus important. One heavy metal of particular interest is lead, a soft, greyish or silver-white metal found in group 14 of the periodic table, with a relatively low melting point (~327.5 °C) and higher density (~11.34 g. cm^{-3}) than most common metals [9]. Lead is a very poisonous metal upon ingestion, which affects almost every part of your body. However, the most affected parts are the nervous system, livers, and kidneys [10]. As industrialization and globalization intensify, water masses end up having traces of this material. Over the years and of recent, there has been work that demonstrates the effectiveness of GO and GO based materials in removing lead ions from water [11–20]. In one study, Azam et al. [11] investigated the lead ion removal efficiency of graphene oxide prepared by modified Hummer's method, from graphite that was derived from waste dry cell battery. The authors determined the rapid ability of GO to remove lead ions from water, whereby 98% removal rates were observed in 20 min, which was attributed to the oxygenated groups on the structure of GO. Upon doing isotherm modelling, the Langmuir isotherm was determined to be accurate at lower temperatures, while the Freundlich isotherm was consistent with the adsorption process at higher temperatures. The resulting maximum adsorption capacity values from these isotherms were 5.80, 54.03, and 51.83 mg g^{-1}, and GO portrayed a re-usability efficiency of six cycles.

In another study, Gomes et al. [12] synthesized graphene oxide from purchased graphite powder, using Hummer's method of synthesis, then investigated its effectiveness in removing lead ions from water. The authors discovered that GO had a high capability of lead ion removal from water, and the Freundlich isotherm was consistent with adsorption process, with a maximum adsorption capacity of 55 mg.g^{-1}. This described a heterogenous adsorption process whereby adsorption takes place on a multilayer basis on the surface of the adsorbent, and possibly both chemical and physical adsorption occurred. Due to the complex behaviour of GO in this application and the ease of availability of graphite, the need to continue exploring the effectiveness of GO to remove lead ions from water arises. This would help to fully understand the adsorption process and optimize it in terms of costs and efficiency. The traditional Hummer's method of synthesis is relatively cost effective and less vigorous, compared to other variations of synthesizing GO. Some of the variations of this method utilize a lot of chemicals, thereby requiring relatively more money to purchase them [21]. Some of these chemicals, like phosphoric acid and nitric acid, react vigorously, which increases the potential for an explosion. Also, some improved methods of GO synthesis upscale the potassium permanganate content added for oxidation, which requires extra sensitivity to not have a vigorous reaction, and thus prolongs the synthesis process. As such, in trying to analyse the most basic GO structure, it would suffice to stick with the Hummer's method of synthesis and commence from that point. As for the type of adsorption experiments that could be used is batch experiments because they reduce the chances of cross contamination of GO back to the water, as it is easily recovered after use, ergo saving time and money The present work aimed to successfully synthesize graphene oxide (GO) from expandable graphite (EG) flakes, contribute to its structure properties by doing Fourier transform infrared spectroscopy (FTIR) X-ray diffraction (XRD), Scanning electron microscopy (SEM) analyses, assess its thermal stability through thermogravimetric analysis (TGA), and test for its effectiveness in removing lead ions (Pb(II)) from water through batch adsorption experiments, Atomic absorption spectroscopy (AAS) and kinetic modelling.

2. Methodology

2.1. Materials

Commercial grade graphite (ES250) was used for the synthesis of GO. It has 90–95% carbon content, an expansion rate of 250–500 cm^3/g at a temperature range between 180 and 300 °C, with more than 80% of its contents having a particle size greater than 300 μm. This graphite was supplied by Qingdao Kropfmuehl Graphite in China, and was received in the form of flakes. Chemicals that were used for the synthesis of GO are the following: Sulphuric acid (H_2SO_4), M_w = 98.1 g/mol, ρ = 1.84 g/cm^3, Assay = 95–99%, Potassium permanganate ($KMnO_4$), M_w = 158.0 g/mol, Appearance: Dark purple needle like crystals, Assay = 99.0%, Hydrogen peroxide (H_2O_2), M_w = 34.0 g/mol, ρ = 1.11 g/cm^3, Assay = 30%, Hydrochloric acid (HCl), M_w = 36.5 g/mol, ρ = 1.16 g/cm^3, Assay = 32%, all supplied by Sigma-Aldrich, South Africa.

2.2. Methods

2.2.1. Functionalization of EG to form GO

The formation of GO proceeded via Hummer's method of functionalizing EG [22]. The stepwise preparation is shown below:

EG flakes (2 *g*) were mixed with $NaNO_3$ (2 *g*) in 50 ml of H_2SO_4 (98%), in a 1 L (1000 ml) volumetric flask. This mixture was kept in an ice bath at 0–5 °C with continuous stirring, for 2 h.

After 2 h, $KMnO_4$ (6 *g*) was added to the suspension very carefully and at a very slow rate, to keep the temperature of the reaction below 15 °C.

The ice bath was removed, and the stirring of the mixture continued at 35 °C until a pasty brownish mixture formed. Further stirring took place for 2 days.

After 2 days, the paste was diluted by adding 100 ml of water very slowly, in a dropwise manner. This increased the reaction temperature to around 98 °C and a visible foam formed, which was brown in colour.

To the solution a further 200 ml of water was added, while continuously stirring, to dilute the mixture again.

The final treatment occurred by the addition of H_2O_2 (10 ml) in order to terminate the reaction. The termination was verified by the appearance of a yellow colour.

The mixture was then purified by washing and centrifugation with 10% HCl and deionized water respectively, for 10 consecutive times.

Then filtration and drying under vacuum took place at room temperature, which resulted in the GO being obtained as a fine powder shown in Fig. 2 below.

2.3. Characterization

2.3.1. Structure, morphology, and thermal degradation properties of GO

The successful attachment of oxygen containing functional groups on EG was confirmed by Fourier-transform infrared (FTIR)-Attenuated total reflectance (ATR) spectroscopy. The analysis took place using the Perkin Elmer Spectrum 100 series spectrometer fitted with a PIKE MiracleTM ATR, equipped with a diamond crystal. In this machine the wavenumber for analysis was set over the range: 650 – 4000 cm^{-1}, using a resolution of 4 cm^{-1} and running a total of 8 scans.

Crystal and interlayer properties of GO and EG were assessed using X-ray diffraction (XRD). The measurements were performed on a Bruker D8 advanced powder diffractometer, with a Cu tube with a wavelength of 1.5418 Å, 40 kV voltage, 40 mA current and 0.6 mm slit size. Bragg's law was used to calculate the interlayer spacing between the different layers of GO and EG, with the aid of Eq. (1) below:

$$n\lambda = 2d\sin\theta \tag{1}$$

where λ represents the wavelength of the x-ray, θ is the scattering angle, d is the interlayer spacing between adjacent atoms, molecules, ions etc., and n is the integer representing the order of the diffraction peak. From there, a calculation of the approximate crystallite size in EG and GO was done following the below Eq. (2), which is called the Scherrer equation [23]:

$$D = \frac{k\lambda}{\beta\cos\theta} \tag{2}$$

where k is the Scherrer constant (shape factor), λ is the wavelength of the X-rays used, β represents the full width at half maximum (FWHM, in radians) and θ the peak positions, in radians The Scherrer constat was obtained from literature as 0.94 [24–26], and the β was determined from the XRD curves.

The morphology and elemental composition of EG and GO were analysed using Scanning electron microscopy (SEM) – Energy dispersive spectroscopy (EDS). This was done on the TESCAN VEGA 3 scanning electron microscope and Oxford X – MaxN EDS, at an acceleration voltage of 15 kV. The samples were not coated with carbon as graphite and graphene oxide already contain large quantities of the element.

For the thermal stability of EG and GO, Thermogravimetric analysis (TGA) was used. The measurements were performed on a Perkin-Elmer STA6000 analyser. As graphite is known to expand upon heating, very low masses of around 6 mg were used for both EG and GO, at a temperature programme of 30 – 600 °C and a nitrogen atmosphere (20 $ml.min^{-1}$ flow rate). These were performed at a heating rate of 10 °C / min.

Fig. 2. Graphene oxide powder obtained by Hummer's method of preparation.

2.3.2. Batch adsorption experiments

Lead nitrate (analytical grade) was used to prepare stock solutions of Pb(II) ions, and batch adsorption experiments of lead ions (adsorbate) on to GO (adsorbent) were conducted in 50 ml glass beakers. Solutions with different initial Pb(II) concentrations (100, 200, 400 and 600 ppm) were deposited into these beakers, together with ~ 0.8005 g GO powder at room temperature, a pH of 7 (adjusted using 0.01 M solutions of NaOH and HCl), and agitated for 24 h. After this period and equilibrium was reached, the solid phase (GO with adsorbed Pb(II)) was separated from the liquid phase (Pb(II) solution) by filtration, and the first 5 ml of filtrated was discarded, as filter paper contains cellulose that might adsorb some lead ions. Then Atomic absorption spectroscopy (AAS), specifically the Flame atomic spectrometer (GBC 909AA), was used to determine the concentration of lead ions in the filtrate. The concentration of lead ions adsorbed (C_a ($mg.L^{-1}$)) on to GO was determined using Eq. (3) shown:

$$C_a = C_0 - C_e \tag{3}$$

where C_o ($mg.L^{-1}$) and C_e ($mg.L^{-1}$) are initial and final concentrations (mg/L or ppm) respectively, of the Pb(II) ions present in the solution before and after adsorption, for a time t. C_e also represents the concentration of Pb(II) present when equilibrium is reached [27]. From this, it followed that the percentage Pb(II) ions removed (R) (%) and the equilibrium adsorption removal quantity (Q_e) ($mg.g^{-1}$), were calculated by Eqs. (4) and (5), respectively:

$$R = \frac{C_0 - C_e}{C_0} \times 100 \tag{4}$$

$$Q_e = \frac{(C_0 - C_e)V}{m} \tag{5}$$

where m is the mass of the adsorbent and V is the volume of the ions solution.

Adsorption isotherm modelling was done to describe the experimental data in terms of the type of adsorption that took place. Three isotherm models were applied, namely: *Langmuir, Temkin* and *Freundlich*.

2.3.2.1. The langmuir isotherm. The Langmuir isotherm [28] model assumes that the adsorption that takes place on the surface of the adsorbent forms a monosaturated layer of adsorbates. It also assumes that there is a constant energy associated with the adsorption process, and no interaction between the adsorbed molecules. This means that all the adsorption sites on the surface of the adsorbent would have the same energy, and the intermolecular forces decrease with an increase in adsorbent surface area/distance from the adsorption surface. The model is described by Eq. (6) below:

$$Q_e = \frac{Q_m K_L C_e}{1 + K_L C_e} \tag{6}$$

where Q_m ($mg.g^{-1}$) is the maximum monolayer adsorption capacity, K_L ($L.mg^{-1}$) is the Langmuir constant related to the energy of adsorption. The linearized form of this equation is represented by Eq. (7):

$$\frac{C_e}{Q_e} = \frac{1}{Q_m} C_e + \frac{1}{Q_m K_L} \tag{7}$$

From Eq. (8), the constants Q_m and K_L are determined from the gradient and y-intercept respectively, of the linear fit of C_e/Q_e against C_e. From here the model expresses a dimensionless constant termed the Separation Factor or Balance parameter, which is determined by the following Eq. (8):

$$R_L = \frac{1}{1 + C_0 K_L} \quad (8)$$

This separation factor value determines the type of adsorption that took place, whereby $0 < R_L < 1$ represents favourable adsorption, $R_L > 1$ is unfavourable adsorption, and $R_L = 0$ is an irreversible adsorption.

2.3.2.2. The temkin isotherm

The Temkin isotherm model [29] consists of a factor that encompasses the interactions between the adsorbent and the adsorbate when adsorption occurs. Eq. (9) is used to describe this model below:

$$Q_e = \frac{RT}{A_T} \ln(B_T C_e) \quad (9)$$

where R (8.314 $J.mol^{-1}.K^{-1}$) is the molar gas constant, T (K) is the temperature, and A_T ($J.mol^{-1}$) and B_T ($L.g^{-1}$) are constants related to the heat of adsorption and the maximum binding energy, respectively. In its linearized form Q_e (on the y-axis) is plotted against C_e (on the x-axis), according to Eq. (10) below:

$$Q_e = \frac{RT}{A_T} \ln + C_e \frac{RT}{A_T} \ln B_T \quad (10)$$

From here, the constants A_T and B_T are determined from the gradient and y-intercept, respectively.

2.3.2.3. Freundlich isotherm

In the Freundlich isotherm model [30] the surface upon which adsorption takes place is believed to be heterogeneous in nature, whereby the active sites and their energies are exponentially distributed. This model is typical for multilayer adsorption processes, which in most cases are a combination of both chemical and physical adsorption (chemisorption and physisorption). The following Eq. (11) is used to define this model:

$$Q_e = K_F C_e^{\frac{1}{n}} \quad (11)$$

where K_F ($mg.g^{-1}$) is the Freundlich constant related to affinity and n is a dimensionless constant related to the type of adsorption (chemisorption if $n < 1$, physisorption if $n > 1$). The model is then linearized to give Eq. (12):

$$\ln Q_e = \frac{1}{n} \ln C_e + \ln K_F \quad (12)$$

Whereby $\ln Q_e$ is plotted against $\ln C_e$, and the constants n and K_F are determined from the gradient and y-intercept, respectively.

3. Results and discussion

3.1. GO synthesis, structure and morphology

3.1.1. FTIR analysis to verify the functionalization of EG to GO

The identification of functional groups that are present in each material can be accurately achieved through infrared spectroscopy. Fig. 3 presents the FTIR spectra of (a) EG and (b) synthesized GO to contrast the functional groups present in the two materials. For EG, there were three distinct regions with wavenumbers: 3791 – 2664 cm^{-1}, 2095 cm^{-1}, and 1810 – 1211 cm^{-1}. The first region (3791 – 2664 cm^{-1}) comprises of a broad peak, and it signified the absorption of moisture by the graphite structure, alluding to its hydrophilic nature. The distinct band at 2095 cm^{-1} is very sharp in shape, representing the -C-H- bending inside the cyclic structure of EG. Then in the last region (1810 – 1211 cm^{-1}) there were a series of overlapped bands, but the significant one was at 1639 cm^{-1}. This was a rather broad band, which is representative of the -C = C- stretching for the conjugated structure of EG.

Then for GO in Fig. 3. (b), there were several newly registered and more distinct bands, as compared to the spectrum of EG. The first peak observed was at 3369 cm^{-1}, which represents the hydroxyl (-O-H) stretching of absorbed water molecules and the presence of chemically bonded hydroxyl (-O-H) groups on GO. It is very important to note that the obtained GO powder was not completely dry as it absorbs moisture from the surroundings. This validates the broadness of this peak and the hydrophilic nature of GO. From there, there was a narrow band at 2926 cm^{-1} and it represents the -CH_2- symmetric stretching in GO. The peak at 1635 cm^{-1} represents the -C = C- stretching when a transition occurs from unoxidized EG to oxidized GO. This peak had shifted by 3 cm^{-1} on the GO spectrum, as compared to its position on the spectrum of EG, thereby validating that a chemical reaction occurred (functionalization of EG to GO). Then there were bands registered at 1724 cm^{-1} and 1166 cm^{-1}, which were due to the -C = O and -C-OH stretching of GO, respectively. These two peaks are a clear indication and validation of the successful attachment and presence Carboxyl groups (-COOH) in the structure of GO. There was also a peak observed at 1040 cm^{-1} and it represents the stretching of the ester (-C-O—C-) group. This band alluded to the fact that the Ester groups was successfully attached to EG during functionalization. Lastly, there was a registered narrow band at 876 cm^{-1}. This peak represents the C—H stretching in the structure of GO. The FTIR results conclusively proved that several oxygen-containing functional groups were successfully attached to EG to convert it to GO. The discussed FTIR results could go a long way in contributing to the ongoing research about the actual functional groups present on the structure of graphene oxide.

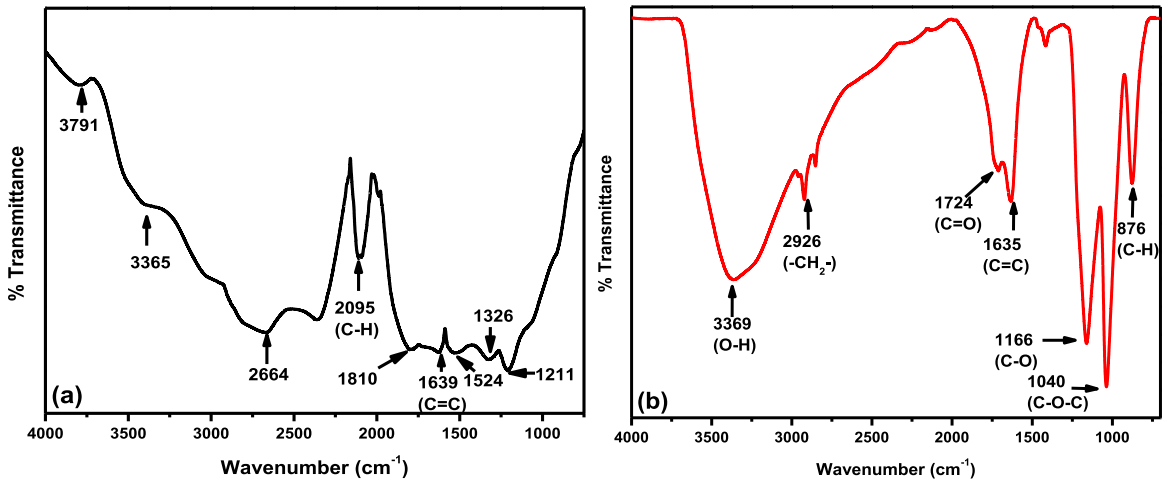

Fig. 3. The Obtained FTIR spectra for (a) EG and (b) GO, showing the addition of oxygen-containing functional groups on the structure of GO from the functionalization of EG.

3.1.2. The crystal properties of EG and GO using XRD measurements

The crystal structure and properties of the synthesized graphene oxide was analysed through XRD. This was done in order to verify the successful functionalization of graphite to graphene oxide and to contribute further to the ongoing research towards the structure of graphene oxide. Fig. 4 presents the XRD diffractograms for expandable graphite (a) and the synthesized graphene oxide (b), and the parameters obtained from using Bragg's law are presented in Table 1. In Fig. 4(a), the expandable graphite exhibited three peaks, at 2theta (θ) values of 25.99 °, 55.56 ° and 87.43 °, respectively. The first peak was sharp and is the main identifying peak of graphite, with a calculated interlayer spacing of 0.3427 nm. This value indicates an almost perfectly ordered structure, which is typical of EG, whereby the layers are orderly and very closely packed to one another. Then the presence of the other two peaks signified a c-axis orientation, which is definitive of a fibre-like structure in EG. The diffractogram of graphene oxide (Fig. 4. (b)) resulted in an extra peak registered at a 2θ position of 7.286 °, in addition to the three other peaks. This is the defining peak for GO, with a calculated interlayer spacing of 1.213 nm. The peak represents and validates the successful addition of oxygen containing functional groups on EG. It also portrays the intercalation of various oxygen-containing molecules in between the GO sheets during synthesis, as the layer spacing increased. The increased interlayer spacing from 0.3427 nm in EG to 1.213 nm in GO indicated that the layers in the GO had opened up, which was the intent when synthesizing GO.

In determining the approximate lateral crystal sizes perpendicular to the plane of the material, the obtained results and parameters were tabulated in Table 2. From the table, the crystallite size obtained for EG was 11.59 nm, whilst GO resulted in an approximate crystallite size of 16.13. The increased size of crystallites for GO as compared to EG, is indicative of the presence and successful addition of oxygen containing functional groups on the layers of GO. This would create an overall enlarged size of the crystallites involved, with the addition of these groups. Also, the crystallite size obtained for GO implies that the surface area of the synthesized GO is a bit larger than that of EG. This is particularly important for adsorption purposes, the higher the surface area of a material then the higher the chances of getting optimal adsorption rates. The enlarged surface area in this case is very much relevant as it is filled with highly adsorptive functional groups, to ensure the effective removal of lead ions from solution. Relatively higher crystallite sizes can also result in effective processability in water, on a general basis. Therefore, this would aid in improving the water intake properties of GO, while maintaining a certain level of endurance and prolonged usage, as the lateral crystal sizes are enhanced. XRD analyses have provided further insight into the crystal behaviour of GO and proved that its synthesis was successful.

Table 1
Bragg's law parameters for the defining peaks of EG and GO, in XRD.

Sample	2θ / °	θ / °	n	λ / nm	d / nm
EG	25.99	13.00	1	0.15418	0.3427
GO	7.286	3.643	1	0.15418	1.213

θ – Scattering angle, λ - Wavelength of the X-ray, n – Order of the diffraction peak, d – Interlayer spacing.

Table 2
XRD parameters for the determination of average crystallite sizes of GO and EG.

Sample	2θ /rad	θ /rad	K	λ /nm	β /rad	D /nm
EG	0.4536	0.2268	0.94	0.15418	0.01283	11.59
GO	0.1272	0.0636	0.94	0.15418	9.006×10^{-3}	16.13

θ – Peak position, K - Scherrer constant, λ - Wavelength of the X-ray, β - full width at half maximum, D - Approximate crystallite size.

3.1.3. Surface morphology and compositional analyses of EG and GO using SEM-EDS

The surface morphology as well as composition of the EG and GO were analysed using SEM-EDS. In Fig. 5, SEM micrographs of EG are displayed, using 60 × magnification ((a) and (c)) and 1000 × magnification ((b) and (d)). At a lower magnification (Fig. 5(a)), the expandable graphite shows sheets with relatively smooth surfaces, with no pores. These sheets appear to generally differ in size although their thickness seems to average the same approximation, as is shown by the images. Zooming into one of the graphite sheets (Fig. 5(b)), the smoothed out and non-porous surface morphology is observed. This observed morphology is typical of graphite as it consists of only carbon atoms, bonded together by strong intra- and intermolecular forces between the carbon atoms. The corresponding layered images (Fig. 5(c) and (d)) show the distribution of the chemical components that are present in expandable graphite flakes. As it was expected, the observed major component in expandable graphite was found carbon. This is shown by the graphite flakes being covered by red in the images, which represents the carbon atom. The carbons in the EG grade used are evenly distributed and bonded throughout the surface and overall structure of graphite. Then there were traces of oxygen found on the surface of graphite, as is shown by the yellow dots on Fig. 5(d). The oxygen might have emanated from the moisture that EG had absorbed from the surroundings, as it is known to be a hydrophilic material.

Then the SEM images of the prepared graphene oxide are shown in Fig. 6, at 60 (a), 500 (b), 1000 (c) and 2000 (d) × magnifications. In Fig. 6(a), the GO seems to show exfoliated sheets, as compared to EG, which provides validation that the GO was successfully synthesized. This

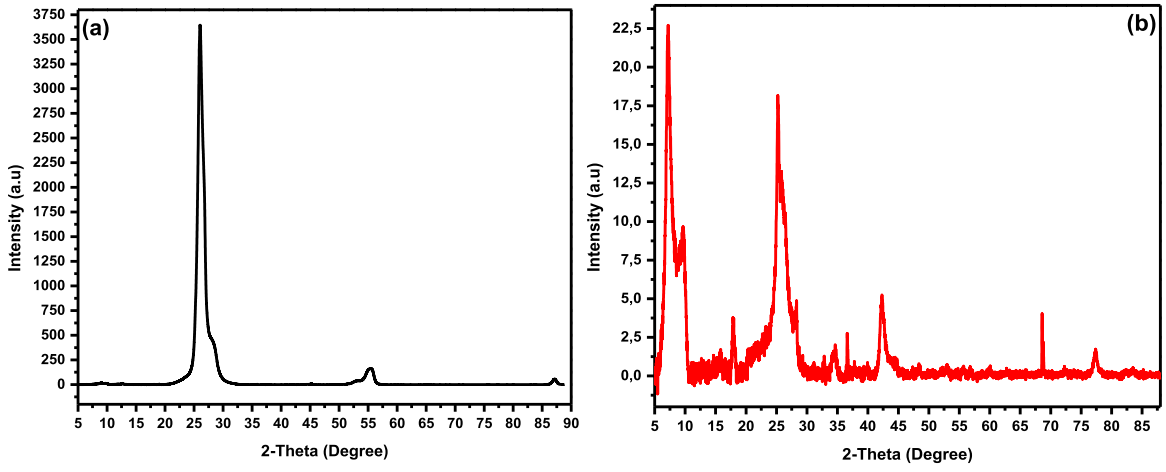

Fig. 4. XRD patterns of (a) EG and (b) GO showing the defining peaks and crystal nature of these materials.

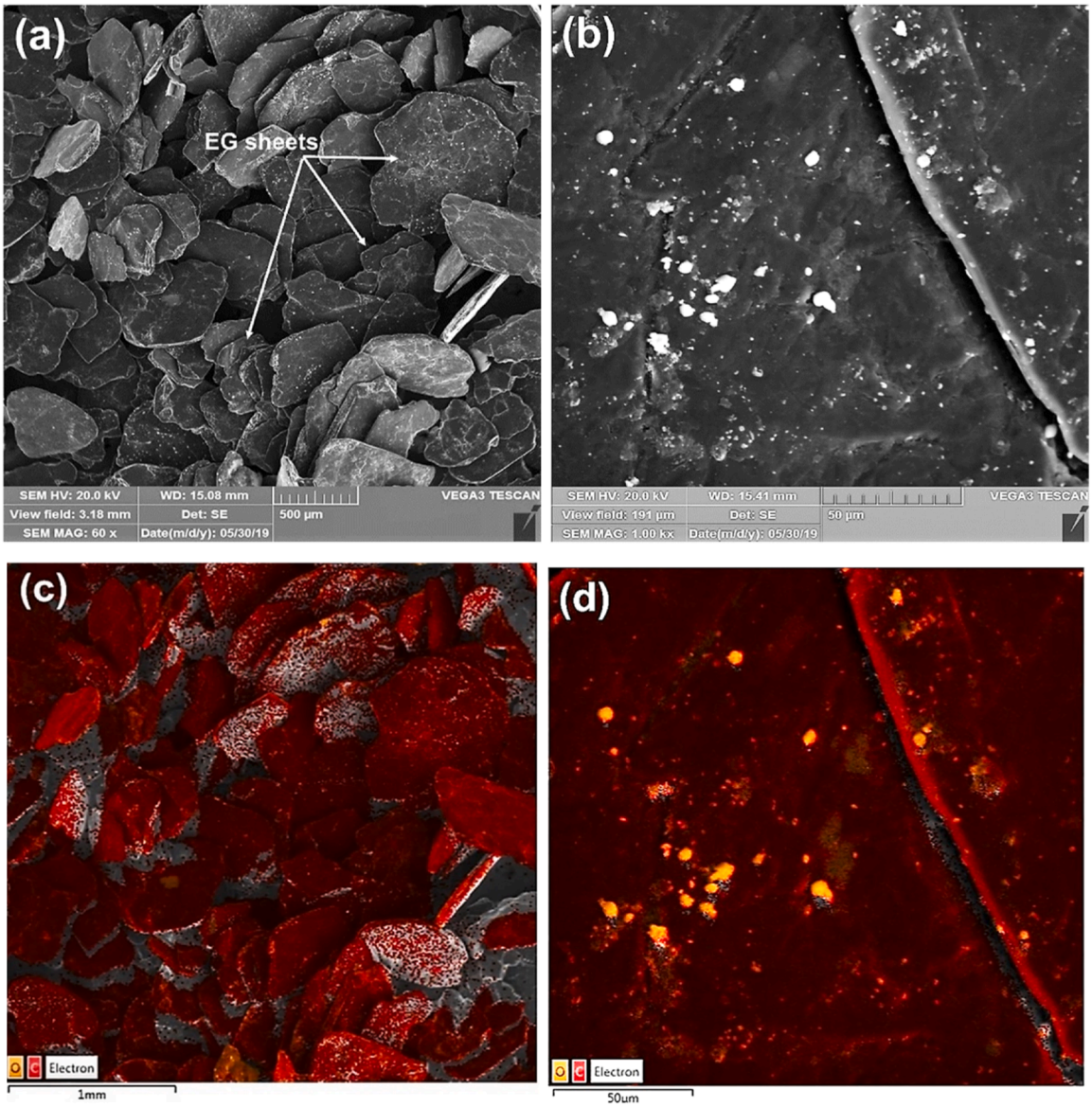

Fig. 5. SEM images and maps of EG at 60 × magnification ((a) and (c)) and 1000 × magnifications ((b) and (d)), to showcase the surface morphology and distribution of elements in EG.

is because the exfoliation of the graphite surface is one of the aims in the synthesis of graphene oxide. The seemingly exfoliated sheets resulted in a wrinkled surface morphology in GO, and this observation is attributed to the successful attachment of oxygen-containing functional groups on GO. As the magnification was increased, the layered nature of GO became apparent in Fig. 6((b), (c) and (d)). Arrow A (Fig. 6(b)) shows the layers present in GO, as well as their arrangement. There are considerable distances observed in between the layers, which validates the increased interlayer spacing observed in XRD. This would allow for increased water intake and metal adsorption capabilities to take place in between and on these layers. From here it is vital to note that some of the layers of EG were showed to widely open during synthesis to form GO, whereas some had remained intact and stacked together in GO, as is shown by Fig. 6((b) and (c). This is owed to the partial addition or lack of oxygen-containing functional groups on some areas of the graphite structure, and the visible wrinkles were areas of this lack of oxidation and/or deformity, causing the layers to not be opened to the same extent. Also, the GO might have absorbed water during synthesis, resulting in some of its layers stacking against each other. This would validate the hydrophilicity of GO, and therefore validate its efficiency in water-based studies. The layers of GO also appeared larger in size, as compared to those of EG, and this was presumed in XRD analyses. The SEM images obtained for GO have served as verification for the calculated results in XRD. This proposed idea of the partial opening of layers and some stacking effect in GO, might work to contribute to the ongoing research into the exact morphology of GO, currently conducted worldwide.

In trying to see the distribution of the components in GO, maps were obtained for each one of the images in Fig. 6, and results are presented in Fig. 7. The maps generally show the presence of carbon (red colour), oxygen (green colour), sulphur (blue colour), potassium (yellow colour) and manganese (purple colour). The oxygen is clearly widely distributed on the GO, as is shown by the green mapping colour that corresponds to oxygen, on the maps. This also serves as confirmation of the successful attachment of oxygen-containing functional groups on graphite, to form graphene oxide. Then there were not so significant traces of potassium (K) and manganese (Mn) here and there, which resulted from the potassium permanganate used to oxidise the graphite structure, and those can be ignored. This means that in areas where these traces appeared the most, the attachment of oxygen-containing groups was a bit less, even

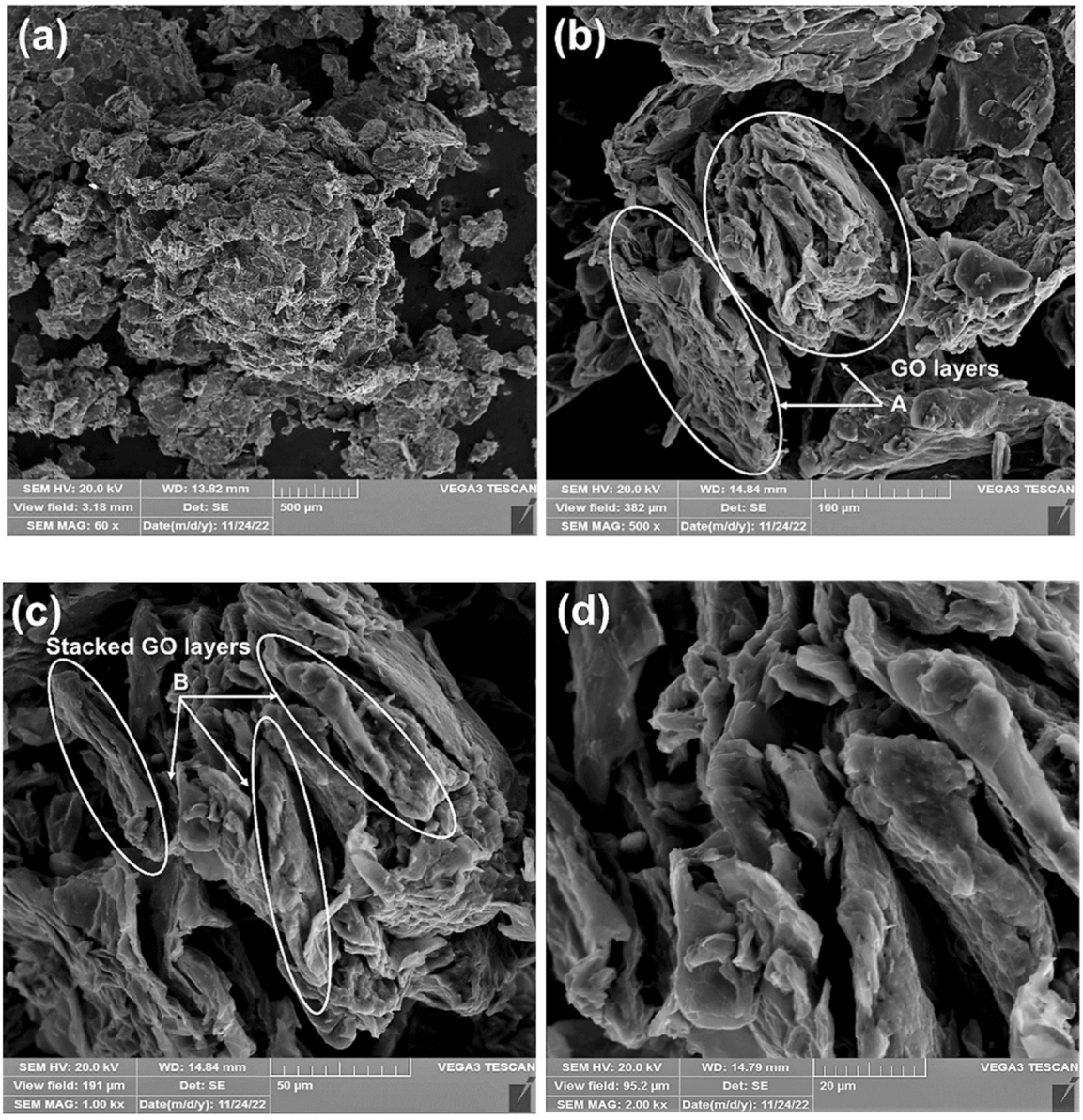

Fig. 6. SEM images of GO at 60 (a), 500 (b), 1000 (c) and 2000 (d) × magnifications, displaying the surface morphology and sheeted nature of GO.

though it still occurred. As the edges and surfaces seem to considerably have oxygen content, it can be assumed that the oxygen containing functional groups were evenly dispersed along the whole surface area of GO. This also contributes to the ongoing research on the distribution and location of these groups. The Hummer's method of synthesis is suggested to distribute the groups evenly, with small traces of Mn and K [22]. The said even distribution of the oxygen-containing functional groups means that these groups are present on both the edges and lateral surfaces of GO [22], and this could work to advantage the adsorption applications, in this study. That is, it is vital to have an attachment of pollutants onto both the edges and the surface of the adsorbent, as it would ensure that the adsorbent is optimized in its adsorption capability. Furthermore, the small traces of sulphur (S) seen were due to the used sulfuric acid during synthesis, and probably the sulfuric acid (H_2SO_4) present in the EG as an intercalation agent that ensures the expansion of graphite [31–33]. This would not disrupt the use of this material in the adsorption of lead ions from water, because sulphur has not been proven to inhibit the adsorption process. The SEM images and maps of GO provided great insight into its proposed morphology, and further ascertained the feasibility of using it in water related research.

From the above findings, EDS spectra were obtained to do the elemental analysis of EG and GO, as shown in Fig. 8. For the elemental analysis of EG (Fig. 8(a)), the significant elemental percentages were that of carbon (83%) and oxygen (12.3%). The compositional ratio in between the mentioned elements is approximately 7:1 respectively for carbon and oxygen. These observations were very much expected, and they serve as validation that the structure of graphite consists mostly of carbon, and that graphite is a hydrophilic material. Then there was a sulphur content of 2.3%, which was probably due to the intercalating agent (H_2SO_4) used when EG was manufactured [31–33], as already mentioned in the preceding discussion. Coming to the spectra of GO (Fig. 8(b)), significant elemental composition changes were observed. Firstly, the carbon content was now 61.4%, whereas that of oxygen settled at 32.1%, with the insignificant elements still present. From these observations it was determined that the ratio between carbon and oxygen (C:O) was calculated to be approximately 2:1. The increased content of oxygen for GO was expected as it signified the successful addition of oxygen-containing functional groups. Then the obtained ratio between the two elements conclusively validates the successful synthesis of GO from EG, as this is the known ratio between carbon and oxygen in

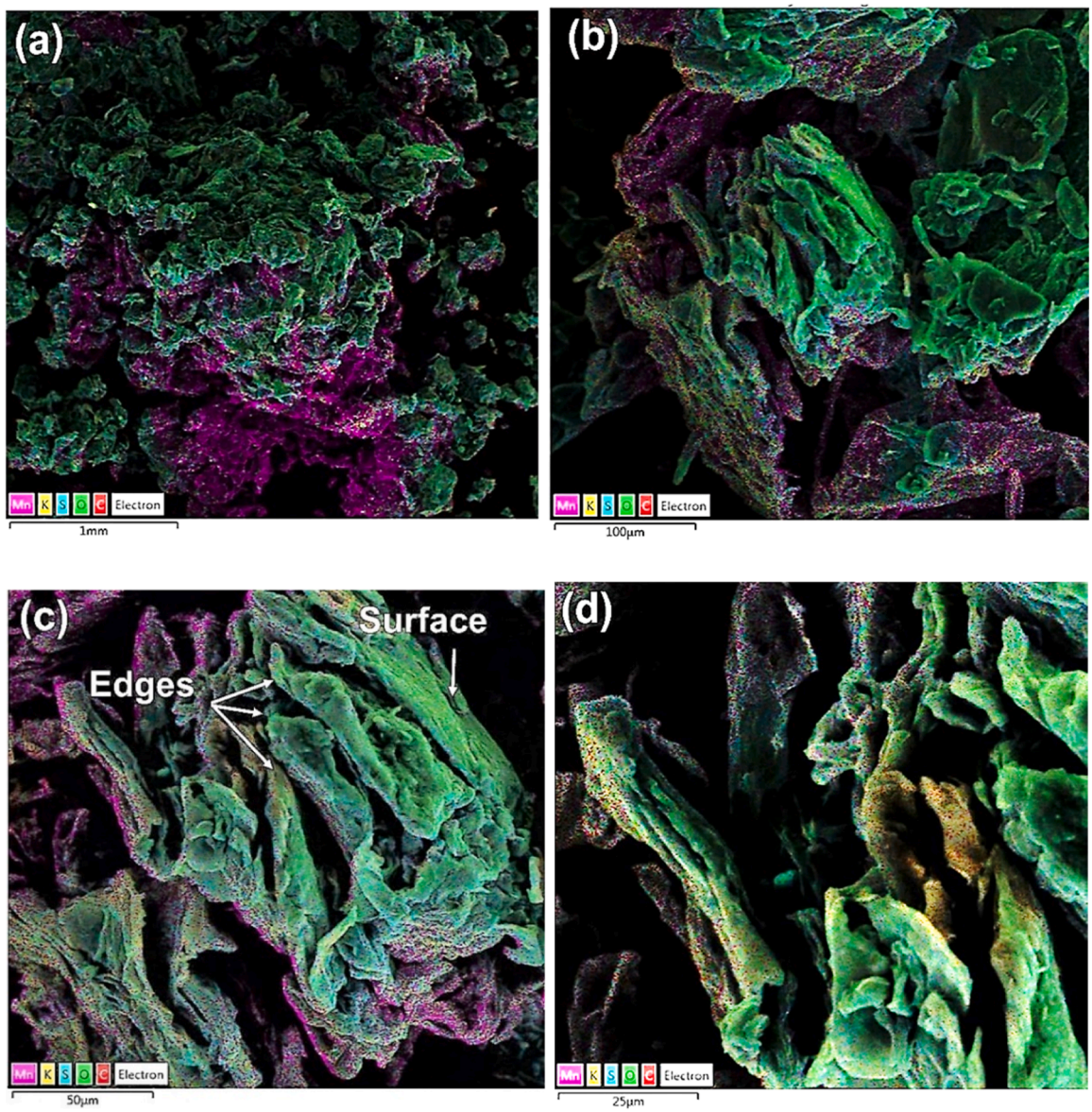

Fig. 7. EDS maps of GO at 60 (a), 500 (b), 1000 (c) and 2000 (d) × magnifications, displaying the extent to which functionalization of EG to GO occurred, as well as elemental distribution on the structure of GO.

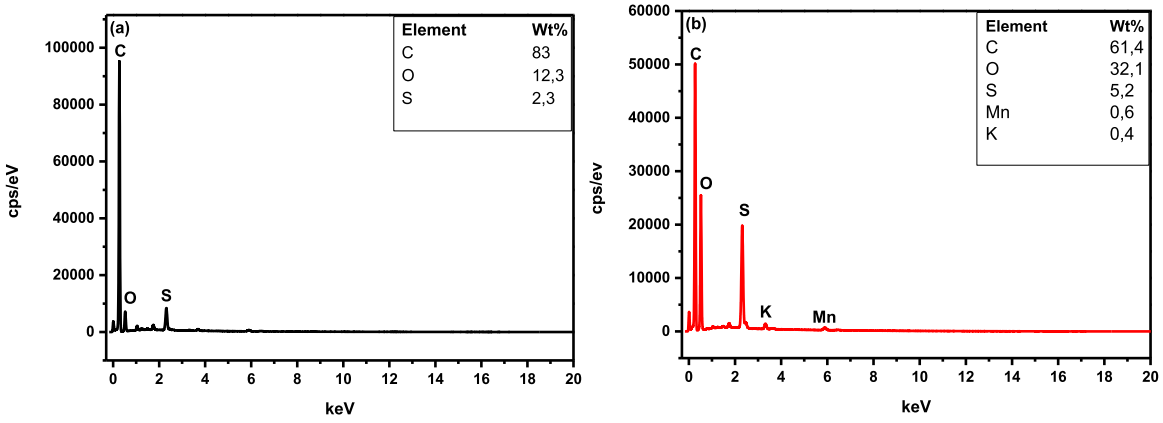

Fig. 8. EDS spectra for EG (a) and GO (b), clearly showing the C:O ratios in the two materials.

graphene oxide.

SEM-EDS was very instrumental in assessing the morphology of EG and GO, giving insight into the proposed distribution of the oxygen-containing functional groups on GO, and verifying that the GO was successfully synthesized from EG. It also highlighted the feasibility of GO being used as a metal adsorbent in water, as made possible by its structure. As GO is still being explored in terms of its structure and properties, any proposed information in its regard should be deemed crucial and therefore be subjected to analysis. This would open way into the usability and reusability of this material in different applications.

3.1.4. The thermal stability analysis of EG and GO using TGA

TGA was used to develop an estimation of the thermal degradation properties of EG and GO, to contrast between the two and further gain insight into the feasibility of applications in water studies. The TGA results are shown in Table 3 displaying the degradation temperatures, as well as Fig. 9, which shows the TGA curves (a) and TGA derivative curves (b) of EG and GO. EG showed one degradation step commencing at 208.3 °C, and with a maximum degradation at 211.3 °C. This step accounted for about 70% of the mass loss, with a char content of approximately 30% remaining. In this decomposition step, the sulphuric acid and carbon in EG are said to undergo a redox reaction, thereby releasing carbon dioxide (CO_2), Water (H_2O) and sulphur dioxide (SO_2) gasses [34–37]. This happens while the previously absorbed water by graphite is being released as well. It has been established that graphite does not degrade at the temperature range used but instead melts at temperatures above 700 °C, hence the presence of the char content [35–37].

GO degraded in three interconnected steps in the temperature ranges: 30 to ~ 100 °C, 100 to ~ 150 and 150 to ~ 350.0 °C respectively, as is depicted by Table 3 and Fig. 9(a). These degradation steps had corresponding maximum degradation temperatures of 65.34, 149.90 and 257.0 °C respectively, as Table 3 and Fig. 9(b) show. The first degradation step represents the removal of water molecules that were previously absorbed during the synthesis of GO, and it accounted for around 20% mass loss. Then the second degradation step represents the thermal degradation of the less stable lactone, hydroxyl, and carboxylic groups from GO. As the degradation steps are conjoined, water is still being released from the hydroxyl groups in this step. While the lactone groups release carbon monoxide and the carboxylic acid groups emit carbon dioxide, this step accounted for about 20% of the total mass loss. Then the last degradation step, accounting for about 24% mass loss, is representative of the thermal decomposition of the more stable ketone and quinone groups attached on GO during functionalization. From this degradation step, it is safe to assume that more ketone and quinone groups were present on GO, compared to the lactone and carboxyl groups, generally. Also, Eigler et al. [38] posited that the structure of GO consists of covalently bonded organosulfate groups, which emanate from the usage of sulphuric acid to oxidize the EG during synthesis, and probably the intercalated H_2SO_4 in EG. These groups are said to also degrade during this third step, resulting in the release of sulphur dioxide. Even though most of the researchers abstain from presenting the presence of these groups, they have been proven to be of vital importance as they help to make graphene oxide more reactive. This would then allow for the tailoring of GO in terms of functionalization, in order to enhance certain properties for applications like adsorption, conductivity and the others. Moreover, this last degradation step of GO occurred at a higher temperature than the corresponding one in the thermal degradation of EG, which shows GO to be more thermally stable than EG. Moving forward, only the EG structure (consisting of only carbon) remained, and no mass loss was recorded on the TGA analysis. This was owed to the fact that the parent structure of graphite does not degrade in the temperature ranges used, and this resulted in a char content remaining of about 36%.

The thermal degradation analyses of GO worked to verify that it was successfully synthesized from EG. Also, these analyses provided insight into the thermal endurance of GO and its usability in elevated temperatures. From this, an optimization of conditions would be explored, whereby temperatures are adjusted where the GO is applied, or the GO would be masked in order to prolong its lifespan. This is particularly important if the graphene oxide is used in water related studies, like metal adsorption, because the water temperature surely fluctuates in nature.

Table 3
TGA degradation temperatures for EG and GO giving an idea of the thermal degradation behaviour of the two materials.

Sample	$T_{1,\ onset}$ / °C	$T_{1,\ max}$ / °C	$T_{2,\ onset}$ / °C	$T_{2,\ max}$ / °C	$T_{3,\ onset}$ / °C	$T_{3,\ max}$ / °C
EG	208.3	211.3	–	–	–	–
GO	30.0	65.3	~100.0	149.9	~150.0	257.0

$T_{1,\ onset}$, $T_{2,\ onset}$, $T_{3,\ onset}$ - Onset degradation temperatures for the first, second and third steps, respectively. $T_{1,\ max}$, $T_{2,\ max}$, $T_{3,\ max}$ – peak degradation maxima temperatures for the first, second and third steps.

3.1.5. The efficiency of GO in adsorbing Pb(II) heavy metal ions from water, using AAS analyses

The ability and extent to which the GO could adsorb lead ions into its surface was analysed through the Atomic absorption spectroscopy. Here the effect of the concentration of lead ions on the adsorption capabilities of GO was analysed, with constant adsorbent masses of approximately 0.800 g. Only this parameter was tested to assess the effectiveness of GO in removing relatively high concentrations of P(II), and to isothermally model the adsorption process. Table 4 presents the findings in this regard, whereby 100, 200, 400 and 600 ppm Pb (II) ion concentrations were used, and the corresponding adsorption parameters were recorded. Generally, GO exhibited exceptionally high adsorption percentages (91.5, 95.1, 97.4 and 98.1%) for all the analysed concentrations, respectively. This is an indication of the high effectiveness and efficacy of GO and its oxygen containing functional groups, as an adsorbent for lead ions in water. Also, from the table it is clearly visible that the relationship between the content of lead ions adsorbed and the initial Pb (II) concentration, is a direct proportion. This means that as the initial lead ion concentration is increased, then the percentage lead ions that is adsorbed by GO also increases. This was very much expected as the increase in adsorbate concentration translates to the increase in lead ions to be adsorbed by the adsorbent. The same trend was observed with the adsorption capacity as the Pb(II) initial concentration was increased, with a maximum capacity of 36.76 $mg.g^{-1}$, at 600 ppm initial concentration. The GO adsorbent was able to remove 98% of the lead ions from water, while operating at a low capacity, showing the feasibility to effectively remove even higher concentrations of lead ions. From here a curve was fitted, showing the relationship between the percentage lead adsorbed and the initial adsorbate concentration, as depicted in Fig. 10. From the curve a clear logarithmic regression was seen, with a relatively accurate fit consisting of two outliers. This curve described a rapid increase in the adsorption percentages in the beginning, then followed by approaching equilibrium towards the end. By extrapolation the curve would probably reach equilibrium before the GO capacity to extract lead ions runs out. This means that probably the GO would get very close to adsorbing a 100% of the lead ions before the adsorbate concentration could be increased to very high values. As a result, it can be assumed that GO alone is capable of effectively adsorbing lead ions up to approximately 800 - 1000 ppm concentrations, before its mass needs to be increased. It is important to note and therefore highlight that the mass used for GO was relatively low, but still yielded very high adsorption percentages. This could ascertain the assumption that graphene oxide would have a high usability in high scale adsorption experiments, given that there is an upscaling of the conditions from the ones conducted in this study. As such, industrial applications of this material for water treatment purposes is feasible to a certain extent.

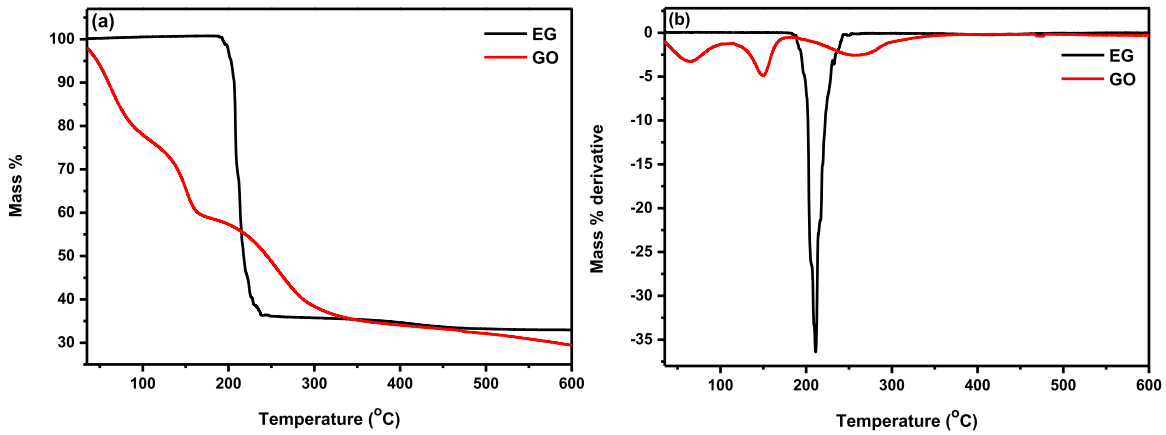

Fig. 9. TGA (a) and TGA derivative (b) curves for EG and GO showing the steps involved in the degradation of these materials, and their maximum degradation temperatures.

Table 4
Parameters obtained from investigating the effect of initial Pb(II) concentration on the adsorption efficiency of GO.

C_i / ppm	m / g	C_a / ppm	% Pb(II) adsorbed	Q_e / mg.g^{-1}
100	0.8005	91.47	91.5	5.634
200	0.8003	190.2	95.1	11.58
400	0.8008	389.7	97.4	24.35
600	0.8005	588.7	98.1	36.76

C_i – Initial Pb(II) concentration, m – Adsorbent (GO) mass, C_a – Concentration of Pb(II) adsorbed, Q_e – Equilibrium adsorption capacity.

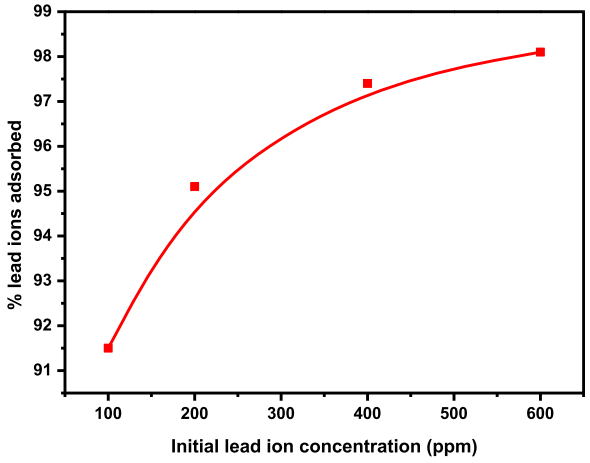

Fig. 10. A plot of the initial lead ion concentration versus% lead ions adsorbed, for ~ 0.8 g adsorbent (GO) mass.

3.1.5.1. Adsorption isotherm modelling. In trying to determine the manner in which the adsorbent (GO) interacted with the adsorbate, isotherm modelling was deployed. This proceeded by using three isotherm models namely: Langmuir, Freundlich and Temkin isotherms. The choice of these isotherms was because they are the widely used and relevant to describe the adsorption of metal ions onto carbonaceous adsorbents. Table 5 presents the parameters obtained for the three isotherm models and the correlation coefficient, while Fig. 11 displays the isotherms fitted for the Langmuir (a), Temkin (b) and Freundlich (c) models.

3.1.5.2. Langmuir isotherm. In Fig. 11(a) the graph was found to be a linear fit with negative values for the slope and the y-intercept. This means that the adsorption that took place does not follow the

Table 5
Parameters obtained from the different models, where GO is the adsorbent.

Model	Equation	Parameters			R^2
Langmuir	$Q_e = \frac{Q_m K_L C_e}{1 + K_L C_e}$	Q_m / mg.g^{-1}	K_L / L. mg^{-1}	R_L	
		−2.241	0.08503	0.01922	0.95846
Temkin	$Q_e = \left(\frac{RT}{A_T}\right)\ln(B_T C_e)$	A_T / J. mol^{-1}	B_T		
		22.77	0.1200		0.8464
Freundlich	$\ln Q_e = \frac{1}{n}\ln C_e + \ln K_F$	K_F/mg.g^{-1}	1/n	N	
		1.760	6.786	0.1474	0.98029

Q_m – Maximum adsorption capacity, K_L – Energy of adsorption constant, R_L – Separation factor, A_T – Heat of adsorption constant, B_T – Maximum binding energy constant, K_F – Affinity constant, n – Adsorption type constant, R^2 – Correlation coefficient.

assumption upon which the Langmuir model is based. That is, the adsorption might not have taken place on a monolayer basis, the surface of the adsorbent might not have been homogenous with uniform forces towards the adsorbate, and lastly there might have been lateral interactions between adsorbed molecules. In providing reasons for the above-mentioned assumptions, the following posits are made: Adsorption cannot take place on a monolayer basis on the surface of GO since oxygen-containing functional groups consist of highly dipolar character, that would first attract the lead ions chemically to the surface of GO, then afterwards attract the ions some more through electrostatic attraction. Secondly, the surface of the adsorbent GO cannot be homogenous with uniform forces (attractive forces with the same magnitude) because there are various oxygen containing functional groups, each with their own attractive forces. Lastly, the lateral interactions between the adsorbed molecules might result from the formed different compounds as the GO surface interacts with the lead ions. This means we would have to consider the presence of the differing oxygen-containing functional groups, and assume that they each form different compounds upon contacting the lead ions. These compounds would then be subjected to lateral interactions like molecular attraction and steric hindrance, depending on their orientation on the surface of GO. From here it can be assumed that the adsorption of lead ions on to the surface of GO occurs via both chemical (chemisorption) and physical (physisorption) means, even though it is chemical for most of the process.

With these findings, the calculated parameters obtained from this model might be considered obsolete to a certain extent, even though they show some accuracy. Just to highlight, the value of R_L was determined to be 0.01922 (Table 5), and since it lies between 1 and −1 then it

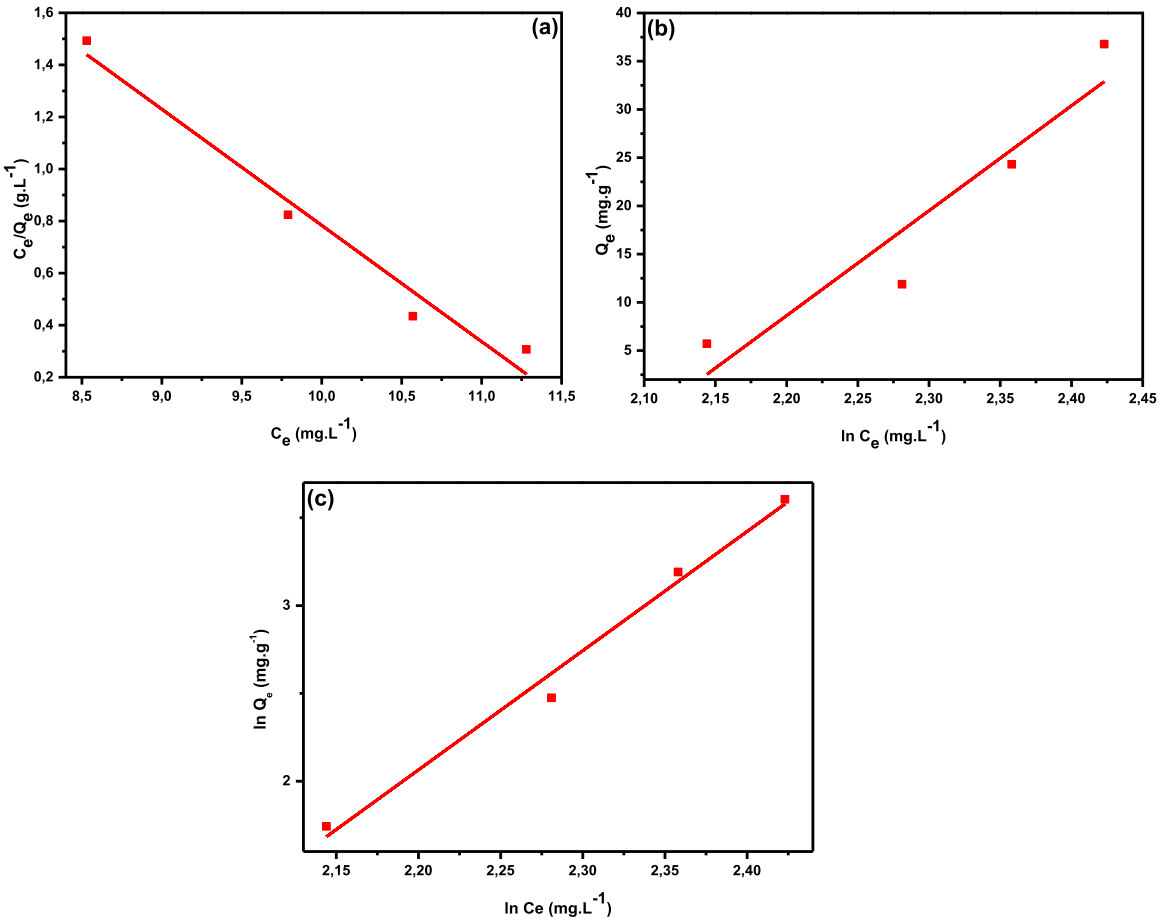

Fig. 11. Langmuir (a), Temkin (b) and Freundlich (c) isotherms for different initial Pb ion concentrations.

indicates a favourable adsorption that is reversible. However, since this model was not viable, perhaps a look into other models would provide further clarity.

3.1.5.3. Temkin isotherm. In using the Temkin isotherm to model the adsorption, the results were presented on the graph in Fig. 11(b) and the parameters obtained in Table 5. The obtained constant for the heat of adsorption (A_T) value was 22.77 $J.mol^{-1}$, suggesting an exothermic adsorption process taking place on the adsorbent GO. This would mean that there is predominantly higher physical adsorption than chemical adsorption of lead ions on to the surface of GO. This is based on the idea that physisorption is generally an exothermic reaction, therefore the assumptions do not have validity. Also, this model would bring the assumption that the energy of adsorption decreases linearly with adsorbent surface area coverage, instead of exponentially. However, the calculated correlation coefficient (R^2) of 0.8464 implied a rather unsatisfactory, or poor regression fit. As such, the Temkin model was deemed unfitting to describe the adsorption process. This is further validated by the fact that this model had been originally formulated for liquid to gas systems and is thus more accurate there. We therefore would need another model to accurately assess the equilibrium adsorption characteristics of Pb(II) ions onto GO.

3.1.5.4. Freundlich isotherm. Then the Freundlich model was applied to try and assess the equilibrium characteristics of Pb(II) adsorption on to the surface of GO. The findings are presented in Table 5 showing the obtained parameters, and Fig. 11(c) which shows the isotherm fit thereof. The fit itself is quite good, with a positive gradient and an R^2 value of 0.98029. This implies that the Freundlich model is accurate in describing the adsorption of lead ions on to the surface of GO. From here, the assumptions made preciously are verified, that the adsorption process was both chemical and physical, as the model describes. The oxygen-containing functional groups might attract the lead ions through chemical bonds, whilst the surface of GO through the same functional groups electrostatically attract the adsorbate. These areas of physical and chemical adsorption are termed adsorption sites, and describe areas of optimal adsorption capacity on the surface of the adsorbent GO. Also, this isotherm conclusively verifies that the adsorption process was on a heterogenous GO surface throughout the surface area of GO, with multilayer adsorption. Furthermore, these results imply that the adsorption sites are exponentially distributed in terms of their energy of adsorption. The physically adsorbed molecules would simplify the process of reusability of the adsorbent, to allow for its reuse. This means that GO, as an adsorbent, can be explored further in terms of desorption and optimization, to reduce fouling. Coming to the parameters obtained (Table 5), the value of n was 0.1474 and it implied that the dominant type of adsorption was chemisorption. This is particularly accurate because most of the oxygen containing functional groups have a high reactivity, as a result of the high electronegativity possessed by oxygen. The Freundlich isotherm was successful in conclusively describing the adsorption process of Pb(II) ions on to the adsorbent GO.

Heterogeneous and multi-layered adsorption is very effective in attaining optimal adsorption capacities. Therefore, the results obtained from this section conclusively verify that GO on its own is an exceptional adsorbent of lead ions from water. We can say that this is owed, for the most part, to the presence of the oxygen containing functional groups on the surface of graphene oxide. However, the layered nature of parent graphite and graphene structures also make for relatively larger surface areas, which would increase the adsorption capabilities as well. This knowledge would add into the already available research done in order

to further optimize this material to effectively clean the water systems.

3.1.5.5. Comparison with literature. Table 6 shows adsorption results from some of the published work in the removal of lead ions by GO and GO based adsorbents, in contrast with the current study. It is apparent that the GO in the current study fends very well in terms of the percentage removal efficiency of Pb(II) ions from water, and this is due to the oxygen-containing functional groups on its structure. The maximum adsorption capacity of this study is a bit low as compared to the other adsorbents outlined in Table 6. This might have been due to the high initial concentrations of lead ions used in this study (around 600 ppm maximum concentration), compared to other studies where lower initial concentrations are utilized (400 ppm maximum concentration). The higher the initial Pb(II) concentration, the more occupied the adsorption sites on the surface area of GO. Furthermore, it has already been explained that the traditional Hummer's method of preparation is relatively quicker and cost efficient. Although some literature has resulted in higher adsorption capacities, the methods used to synthesise GO might have not been cost effective, with prolonged synthesis periods. This means that the cost-to benefit of the traditional Hummer's method of preparation, could be a bit higher and therefore worth exploring. Moreover, in adsorption studies, reusability is important so that adsorbents can effectively be re-used to save money and time. A high adsorption capacity describes a high rate of adsorption, which might cause the adsorbent to experience fowling quicker, and thus limit reusability. It is always important to have materials that can exhibit very high adsorption percentages while operating at low capacities, to be able to prolong the usage of these materials. This would justify the obtained adsorption capacities in this work, inferring that the GO in this study might have a higher re-usability capacity, due to presumed non-saturation. Nonetheless, the removal efficiency of the adsorbent in this study shows that it is capable of effectively removing lead ions at concentrations going up to 600 ppm. It seems, as well, that the isotherm of adsorption alternates between the Freundlich and Langmuir isotherms. More specifically, Table 6 shows that the Freundlich isotherm is mostly accurate where only GO is used as an adsorbent, whereas in cases where GO-based adsorbents are used then the Langmuir isotherm would accurately describe the adsorption. These findings imply that the utilization of GO on its own to remove lead ions from water, almost always results in a heterogenous and multilayered adsorption process. This makes sense because the oxygen-containing functional groups on the structure of GO are highly reactive, and electronegative. This would encourage both chemisorption and physisorption whereby the lead ions would first form an intramolecular (bonding) attraction with the oxygen groups (binding sites) on GO. Then afterwards an intermolecular (electrostatic) interaction would attract these lead ions to the GO, due to the high electronegativity, thereby exhibiting a multilayered type of adsorption. Then when composites are formed with GO, the components of the constituents of these composites might react with the GO, thereby allowing for a monolayer adsorption process that is either chemical or physical, depending on the components involved and the adsorption conditions.

Table 6
Literary results of Pb(II) adsorption using GO and GO based adsorbents in comparison with the ones from this study.

Adsorbent	% Pb(II) removal	Q_m / mg.g^{-1}	Isotherm model	Reference
GO	98.9	51.83	Freundlich	Azam et al. [11]
GO	100	59	Freundlich	Gomes et al. [12]
GO	98	60	–	Raghubanshi et al. [13]
PEI/GO	79	64.94	Freundlich	Al-Yaari et al. [14]
nano-GO	95	1896	Freundlich	Parsa et al. [15]
Salen-GO	~98	68	Langmuir	Brohi et al. [16]
GO/CNTs	95–100	98	Langmuir	Musielak et al. [17]
GO/pal	50	106.6	Langmuir	Zeng et al. [18]
rGO-PDTC/Fe_3O_4	–	147.1	Langmuir	Fu et al. [19]
TEA-GO-FE	–	121.5	Langmuir	Ren et al. [20]
GO	98.1	36.8	Freundlich	This work

Q_m – Maximum adsorption capacity at highest Pb(II) initial concentration, PEI/GO – Polyethyleneimine-grafted graphene oxide, nanomodified graphene oxide, Salen-GO – Salen functionalized GO, GO/CNTs – Graphene oxide/carbon nanotubes, GO/Pal – Graphene oxide/palygorskite composite, rGO-PDTC/Fe_3O_4 – dithiocarbonate-modified magnetic reduced graphene oxide, TEA-GO-FE – Magnetic nano-Fe_3O_4/triethanolamine/GO composite.

As graphite can be obtained from various sources, with low costs, exploring the synthesis of GO to remove heavy Pb(II) from water introduces a cost effective approach to alleviating lead poisoning. Also, the cited literature in Table 6 mostly reports on reusability cycles of approximately 5 times for GO adsorbents, meaning that it is a sustainable adsorbent. The findings of this section worked to validate the effectiveness of GO in removing lead ions from water.

4. Conclusion

This work aimed to successfully synthesize graphene oxide, contribute to the current knowledge on its structure, morphology, thermal degradation properties, as well as to assess its effectiveness in removing lead ions from water. The graphene oxide was shown to be successfully synthesized by the Hummer's method, and this was verified by the FTIR analyses. Absorption bands at 3369, 1724, 1166, 1040 cm^{-1} for GO verified the addition and presence of oxygen containing functional groups, thereby validating the success in synthesizing GO.

In crystal structure analyses, GO exhibited a newly formed significant peak at 7.286 ° on XRD, which was not present for expandable graphite. This peak, together with the calculated interlayer spacing of 1.213 nm (from 0.3427 nm belonging to EG) were characteristic of the theoretical structure of GO. It also showed that the layers had been successfully opened, such that they can be used for applications in adsorption and other applications. Then the crystallite size determination resulted in an increase in crystallite size from EG (11.59 nm) to GO (16.13 nm). These observations brought about the assumed conclusions that the GO layers that the oxygen containing functional groups were successfully added. XRD analyses was successful in describing the crystal structure of GO.

SEM analyses in this case were also very successful in describing the surface morphology of GO, confirming some assumptions made from XRD observations, and proving that GO has been successfully synthesized. Firstly, the smooth surfaces of EG as compared to the exfoliated ones on GO indicated the success in chemical exfoliation of EG to form GO. From here, the successful attachment of oxygen containing functional groups was verified by the wrinkled texture on GO images, as well as its 2:1 ratio obtained between C and O in elemental analysis. Then the maps were very helpful in determining that the oxygen groups were widely and fairly distributed on GO, on both the edges and the surfaces. This information could go a long way into assessing the property control of GO during its synthesis, as it is still being continuously explored. SEM results were very instrumental in taking us a step further into understanding the morphology of GO.

With the structure and morphology understood, the thermal decomposition properties were then assessed. The TGA analyses in this regard determined that EG thermally degrades at 208.3 °C, whilst GO follows three distinct steps commencing at approximately 30, 100 and 150 °C. What is worth noting, as a basis of conclusion, in this case is that GO is a very hydrophilic material, and that reduces its thermal stability or endurance on a general basis. However, its thermal stability is still higher than that of EG, showing its ability to be thermally tailored and necessitating the research towards further improving its thermal stability.

The adsorption capabilities of GO were assessed for Pb(II) ions in water, with the usage of AAS in different lead ion concentrations. The

results in this case brought about the conclusion that GO is a very good adsorbent of lead metal ions in solution, with the highest absorbed percentage of 98.1%, at 600 ppm adsorbate concentration. This is a very high adsorption capacity, and is worth exploring GO further in terms of other properties that affect adsorption, as well as its optimization as an adsorbent. When modelling the adsorption using isotherms, the Freundlich isotherm described the adsorption better, as was validated by the correlation coefficient value of 0.98029. This influenced the conclusions that adsorption was taking place on a heterogenous surface that has a fair distribution of adsorption sites. The type of adsorption that took place between the GO and lead ions was concluded to be both chemical and physical, with the domination of the chemical type. These conclusions are very vital should we wish to further understand the adsorption behaviour, or optimize the adsorption process.

With the findings of this work, further analyses could be done into understanding the structure of GO and tailoring it for specific applications. The material itself would not be practical in its industrial usage as an adsorbent of heavy metals, therefore it would need to be physically altered to achieve this. This can be done by masking it to prolong its lifespan and help improve its thermal stability. The masking can be done with polymers that are biodegradable, and this work intends to head in that direction.

CRediT authorship contribution statement

L.S. Mokoena: Writing – review & editing, Writing – original draft, Methodology, Investigation, Formal analysis. **J.P. Mofokeng:** Writing – review & editing, Visualization, Validation, Supervision, Software, Resources, Project administration, Methodology, Investigation, Funding acquisition, Formal analysis, Conceptualization.

Declaration of competing interest

The authors declare that they have no known competing financial interests or personal relationships that could have appeared to influence the work reported in this paper.

Data availability

Data will be made available on request.

Acknowledgements

The authors would like to acknowledge the Council for Scientific and Industrial Research (CSIR) (Grant number: SS-GEN-HR-009 REV 01 2011), and the Sasol Inzalo Foundation (SAIF), both in South Africa, for the financial support to see this research through.

References

[1] V. Nebol'Sin, V. Galstyan, Y. Silina, Graphene oxide and its chemical nature: multi stage interactions between the oxygen and graphene, Surf. Interfaces. 21 (2020) 1–24, https://doi.org/10.1016/j.surfin.2020.100763.
[2] U. Hofmann, H. Rudolph, Uber die Saurenatur und die methylie rung von graphitoxyd, Ber. Dtsch. Chem (A and B Seri). 72 (1939) 754–771, https://doi.org/10.1002/cber.19390720417.
[3] G. Ruess, Uber das graphitoxyhydroxyd (Grapitoxyd), Monatsh. Chem. 76 (1947) 381–417, https://doi.org/10.1007/BF00898987.
[4] W.S. Schols, H.P. Boehm, Untersuchungen am graphitoxid. VI.Betrachtungen zur truktur, J. Inorg. Gen. Chem. 369 (1969) 327–340, https://doi.org/10.1002/zaac.19693690322.
[5] T. Nakajima, Y. Matsuo, Formation process and structure of graphite oxide, Carbon N Y 32 (1994) 469–475, https://doi.org/10.1016/008-6223(94)90168-6.
[6] A. Lerf, H. He, M. Forster, J. Klinowski, Structure of graphite oxide revisited, J. Phys. Chem. B. 102 (1998) 4477–4482, https://doi.org/10.1021/0P9731821.
[7] A. Jirickova, O. Jankovsky, Z. Sofer, D. Sedmidubsky, Synthesis and applications of graphene oxide, Materials (Basel) 15 (2022) 1–21, https://doi.org/10.3390/ma15030920.
[8] L.S. Mokoena, J.P. Mofokeng, A review on graphene (GN) and graphene oxide (GO) based biodegradable polymer composites, and their usage as selective adsorbents for heavy metals in water, Materials (Basel) 16 (2023) 1–29, https://doi.org/10.3390/ma16062527.
[9] N. Kozyrev, V. Gordeev, Thermodynamic characterization and equation of state for solid and liquid lead, Metals (Basel) 12 (2021) 1–19, https://doi.org/10.3390/met12010016.
[10] A. Wani, A. Ara, J. Usmani, Lead toxicity: a review, Interdiscip. Toxicol. 8 (2015) 55–64, https://doi.org/10.1515/intox-2015-0009.
[11] G. Azam, H. Kabir, A.A. Shaikh, S. Ahmed, M. Mahmud, S. Yasmin, A rapid and efficient adsorptive removal of lead from water using graphene oxide prepared from waste dry cell battery, J. Wat. Proc. Eng. 46 (2022) 1–12, https://doi.org/10.1016/j.jwpe.2022.102597.
[12] B.F.M.L. Gomes, C.M.B. de Araujo, B.F. do Nascimento, E.M.P. de Luna Freire, M. A. Da Motta Sobrinho, M.N. Carvalho, Synthesis and application of graphene oxide as a nanosorbent to remove Cd(II) and Pb(II) from water: adsorption equilibrium, kinetics and regeneration, Environ. Sci. Pollut. Res. 29 (2022) 17358–17372, https://doi.org/10.1007/s11356-021-16943-3.
[13] H. Raghubanshia, S.M. Ngobenia, A.O. Osikoyaa, N.D. Shootoa, C.W. Dikioa, E. B. Naidooa, E.D. Dikioa, R.K. Pandeyb, R. Prakash, Synthesis of graphene oxide and its application for the adsorption of Pb^{+2} from aqueous solution, J. Ind. Eng. Chem. 47 (2017) 169–178, https://doi.org/10.1016/j.jiec.2016.11.028.
[14] M. Al-Yaari, T.A. Saleh, Removal of Lead from wastewater using synthesized polyethyleneimine-grafted graphene oxide, nanomaterials 13 (2023) 1–21, https://doi.org/10.3390/nano13061078.
[15] N. Parsa, H. Hezai, Removal of lead ions from aqueous solutions using melamine-modified nano graphene oxide, Avicenna. J. Environ. Health. Eng. 7 (2020) 55–65, https://doi.org/10.34172/ajehe.2020.09.
[16] R.O.Z. Brohi, M.Y. Khuhawar, R.B. Mahar, Graphene oxide functionalized with a Schiff base for the removal of Pb(II) ions from contaminated water: experimental and modeling approach, J. Chem. Technol. Biotechnol. 95 (2020) 1694–1704, https://doi.org/10.1002/jctb.6362.
[17] M. Musielak, A. Gagor, B. Zawisza, E. Talik, R. Sitko, Graphene oxide/carbon nanotube membranes for highly efficient removal of metal ions in water, ACS Appl. Mater. Interfac. 11 (2019) 28582–28590, https://doi.org/10.1021/acsami.9b11214.
[18] W.J. Zeng, C.Y. Wang, Y.H. Wang, H.M. Guo, Y. Huang, X.L. Zhang, Facile synthesis of graphene oxide/palygorskite composites for Pb(II) rapid removal from aqueous solutions, Wat. Sci. Technol. 80 (2019) 989–997, https://doi.org/10.2166/wst.2019.345.
[19] W. Fu, Z. Huang, Magnetic dithiocarbamate functionalized reduced graphene oxide for the removal of Cu(II), Cd(II), Pb(II) and Hg(II) ions from aqueous solution: synthesis, adsorption and regeneration, Chemosphere 209 (2018) 449–456, https://doi.org/10.1016/j.chemosphere.2018.06.087.
[20] H.S. Ren, Z.F. Cao, X. Wen, S. Wang, H. Zhong, Z.K. Wu, Preparation of a novel nano-Fe_3O_4/triethanolamine/GO composites to enhance Pb^{2+}/Cu^{2+} ions removal, Environ. Sci. Pollut. Res. 26 (2019) 10174–10187, https://doi.org/10.1007/s11356-019-04316-w.
[21] J. Liu, C. Shuping, L. Yanan, Z. Bijing, Progress in preparation, characterization, surface functional modification of graphene oxide: a review, J. Saudi Chem. Soc. 26 (2022) 1–29, https://doi.org/10.1016/j.jscs.2022.101560.
[22] B. Paulchamy, G. Arthi, B. Lingnesh, A simple approach to stepwise synthesis of graphene oxide nanomaterial, J. Nanomed. Nanotechnol. 6 (2015) 1–4, https://doi.org/10.4172/2157-7439.1000253.
[23] R. Sharma, N. Chadha, P. Saimi, Determination of defect density, crystallite size and number of graphene layers in graphene analogues using X-ray diffraction and Raman spectroscopy, Indian J. Pure Appl. Phys. 55 (2017) 625–629.
[24] N. Khaliesah, K. Azhari, M.A. Bustam, P. Pre, Hamon L, Indexing PXRD structural parameters of graphene oxide-doped metal-organic frameworks, Int. J. Recent. Technol. Eng. 8 (2019) 550–553, https://doi.org/10.35940/ijrte.B1115.0982S919f.
[25] D.R. Chowdhury, C. Singh, A. Paul, Role of graphite precursor and sodium nitrate in graphite oxide synthesis, ACS Advances 4 (2014) 15138–15145, https://doi.org/10.1039/c4ra01019a.
[26] N. Kumar, V.C. Srivastava, Simple synthesis of large graphene oxide sheets via electrochemical method coupled with oxidation process, ACS Omega 3 (2018) 10233–10242, https://doi.org/10.1021/acsomega.8b01283.
[27] T. Guo, C. Bulin, Z. Ma, B. Li, Y. Zhang, B. Zhang, R. Xing, X. Ge, Mechanics of Cd (II) and Cu(II) adsorption onto few-layered magnetic graphene oxide as an efficient adsorbent, ACS Omega 6 (2021) 1635–16545, https://doi.org/10.1021/acsomega.1co1770.
[28] I. Langmuir, The constitution and fundamental properties of solids and liquids. Part 1. solids, J. Am. Chem. Soc. 38 (1916) 2221–2295, https://doi.org/10.1021/ja022689002.
[29] M. Temkin, V. Pyzhev, Kinetics of ammonia synthesis on promoted iron catalysts, Acta Physicochimica. U.R.S.S 12 (1940) 327–356.
[30] H. Freundlich, Over the adsorption in solution, J. Phys. Chem. 57 (1906) 385–471.
[31] J. Huang, Q. Tang, W. Liao, G. Wang, W. Wei, C. Li, Green preparation of expandable graphite and its application in flame-resistance polymer elastomer, Ind. Eng. Chem. Res. 56 (2017) 5253–5261, https://doi.org/10.1021/acs.iecr.6b04860.
[32] J. He, M. Yuan, H. Ren, T. Song, Y. Zhang, The electrochemical preparation and characterization of sulfur-free expanded graphite, J. Chem. Sci. 135 (2023) 1–7, https://doi.org/10.1007/S12039-023-02138-5.

[33] B. Gurzeda, P. Krawczyk, Electrochemical formation of graphite oxide from the mixture composed of sulfuric and nitric acids, Electrochemica. Acta 310 (2019) 96–103, https://doi.org/10.1016/j.electacta.2019.04.088.
[34] S. Duquesne, M.Le Bras, S. Bourbigot, R. Delobel, G. Camino, B. Eling, C. Lindsay, T. Roles, Thermal degradation of polyurethane and polyurethane/expandable graphite coatings, Polym. Degrad. Stab. 74 (2001) 493–499, https://doi.org/10.1016/S0141-3910(01)00177-X.
[35] A. Bannov, A. Ukhina, E. Maksimovskii, I. Prosanov, A. Shestakov, N. Lapekin, N. Lazarenko, P. Kurmashov, M. Popov, Highly porous expanded graphite: thermal shock vs. programmable heating, Materials (Basel) 14 (2021) 1–17, https://doi.org/10.3390/ma14247687.
[36] G. Zhang, M. Wen, S. Wang, J. Chen, J. Wang, Insights into thermal reduction of the oxidized graphite from the electro-oxidation processing of nuclear graphite matrix, RCS Advan 8 (2018) 567–579, https://doi.org/10.1039/C7RA11578D.
[37] C. Chen, W. Yen, H. Kuan, C. Kuan, C. Chiang, Preparation, characterization and thermal stability of novel PMMA/expandable graphite halogen-free flame retardant composites, Polym. Compos. 31 (2010) 18–24, https://doi.org/10.1002/pc.20787.
[38] S. Eigler, C. Dotzer, F. Hof, W. Bauer, A. Hirsch, Sulfur species in graphene oxide, Chemistry (Easton) 19 (2013) 9490–9496, https://doi.org/10.1002/chem.201300387.